

# Continuous description of lattice discreteness effects in front propagation

BY MARCEL G. CLERC<sup>1,\*</sup>, RICARDO G. ELÍAS<sup>1</sup> AND RENÉ G. ROJAS<sup>2</sup>

<sup>1</sup>*Departamento de Física, Facultad de Ciencias Físicas y Matemáticas, Universidad de Chile, Casilla 487-3, Santiago, Chile*

<sup>2</sup>*Instituto de Física, Pontificia Universidad Católica de Valparaíso, Casilla 4059, Valparaíso, Chile*

Models describing microscopic or mesoscopic phenomena in physics are inherently discrete, where the lattice spacing between fundamental components, such as in the case of atomic sites, is a fundamental physical parameter. The effect of spatial discreteness over front propagation phenomenon in an overdamped one-dimensional periodic lattice is studied. We show here that the study of front propagation leads in a discrete description to different conclusions than in the case of its, respectively, continuous description, and also that the results of the discrete model, can be inferred by effective continuous equations with a supplementary spatially periodic term that we have denominated *Peierls–Nabarro drift*, which describes the bifurcation diagram of the front speed, the appearance of particle-type solutions and their snaking bifurcation diagram. Numerical simulations of the discrete equation show quite good agreement with the phenomenological description.

**Keywords:** front propagation; fronts interaction; nonlinear waves

## 1. Introduction

The description of mesoscopic or macroscopic matter—matter composed of a large number of microscopic constituents—is usually done using a small number of coarse-grained or averaged variables. To take into account the interaction of the fundamental constituents of the system, the space is partitioned in a large number of cells or regions. The size of these cells is small when compared with the system volume and large with respect to the microscopic scales. Hence, the system is described as an *extended system*, that is, each cell is described by its respective coarse-grained variables—the local dynamics—and the processes of interaction or transport of physical observables between the cells are described by the flows associated with the coarse-grained variables. Consequently, the evolution of these variables is given by a discrete set of ordinary differential equations. This reduction is possible owing to a separation of space–time scales, which allows a description in terms of the slowly varying variables. This is the usual theoretical framework to describe the motion of atoms in a crystal (see the review

\*Author for correspondence ([marcel@dfi.uchile.cl](mailto:marcel@dfi.uchile.cl)).

One contribution of 17 to a Theme Issue ‘Nonlinear dynamics in meso and nano scales: fundamental aspects and applications’.

of Flach & Willis [1] and references therein), where descriptions based on quantum mechanics are completely unmanageable because of the complexity of the number of components concerned. However, when the separation of scales between the microscopic and macroscopic variables is large enough, the matter is usually described by partial differential equations, which are the continuum counterpart description of finite-difference equations. Therefore, the coarse-grained variables are promoted to spatio-temporal fields. This is the case, for example, in fluid dynamics, electromagnetism, population dynamics, elasticity, nonlinear optics and chemical reactions to mention a few. It is in this context of continuous media that the concept of nonlinear coherent excitations or macroscopic particle-type solutions or localized states in extended systems has emerged. The paradigmatic examples of macroscopic coherence state are solitons emerging in the context of fluid dynamics and Hamiltonian systems [2]. Solitons arise from a robust balance between dispersion and nonlinearity.

In multi-stable macroscopic systems—systems that exhibit different equilibria for the same value of the control parameters—coherent states emerge that asymptotically connect different equilibria states, usually called *fronts*, *domain walls* or *wavefronts* [3,4]. Generically, these domain walls are moving, and this type of behaviour is called front propagation. The concept of front propagation emerged in the field of populations dynamics [5,6], and the interest in this type of phenomenon has been growing steadily in chemistry, biophysics, physics and mathematics. In physics, front propagation plays a central role in a large variety of situations, ranging from reaction diffusion models to general pattern-forming systems (see Pismen [4] and the review of Cross & Hohenberg [7] and references therein). From the point of view of dynamical systems theory, in one-dimensional spatial dimension a front is a nonlinear solution that is identified in the co-moving frame system as a heteroclinic orbit linking two spatially extended states [4]. The dynamics of the interface depends on the nature of the states that are connected. If one considers stable uniform equilibrium states, these domain walls are characterized by propagation at a constant speed, which is proportional to the energy difference between equilibrium states [3,4]. The dynamics of these extended bistable systems is characterized by the display of moving interfaces connecting two stable states, the so-called *normal fronts* [8,9]. There exist isolated points in parameter space for which the front is motionless, which is usually called the Maxwell point, and is the point for which the two states have exactly the same energy [10]. A different situation is that of a front connecting a homogeneous and a periodic state, for which there exists a finite region in the parameter space where the front is motionless, called the *pinning range* [11]. In this case, the pinning–depinning transition is expected to occur as a result of the competition between a symmetry breaking of the global energy that tends to favour the front propagation in one direction, and spatial modulations that tend to block the front propagation by introducing local potential barriers. This can be explained by single model describing the dynamics of the core of the front [12,13]. Depending on the dominant effect, the front can either stay motionless, i.e. blocked in the pinning range, or propagate with periodic leaps to the right or to the left when the control parameters are out of the pinning range. Starting from a critical value of the control parameter, the pinning–depinning transition occurs by the disappearance of the motionless front solution.

All the previous rich theoretical descriptions of coherent states change dramatically when the discrete nature of the system under study is relevant. For example, models describing microscopic phenomena in physics, in particular in solid-state physics, are inherently discrete, with the lattice spacing between the atomic sites being a fundamental physical parameter. In this context, the characteristic length of the lattice is of the order of nanometres. The discreteness effects may modify severely the dynamics of the front propagation even in the framework of the simplest models (see the pioneering works of Ishimori & Munakata [14] and Peyrard & Kruskal [15]). The relevant physical contexts can be quite diverse, including hydrogen-bonded chains [16], calcium release waves in living cells [17–19], reaction fronts in chains of coupled chemical reactors [20–22], arrays of coupled diode resonators [23], semiconductor superlattices [24], discontinuous propagation of action potential in cardiac tissue [25–27], arrays of autocrine cells [28], superconductivity in Josephson junctions [29], nonlinear optics and waveguide arrays [30] and the dynamics of neuron chains [31] to mention a few. The dynamics of all these systems is mainly driven by their inherently discrete nature. Hence, understanding the role of discreteness becomes of crucial relevance.

Most of the theoretical works on the spatial discreteness effect over the front propagation have been developed in the framework of Hamiltonian systems [15]. One of the well-known effects in dissipative discrete systems is the propagation failure [32], that is, the front is motionless as a consequence of the discreteness of the systems under study. To take advantage of widespread calculation methods of partial differential equations and developing a qualitative intuition of dynamical behaviours of discrete models, we attempt to circumvent the spatial discreteness effect over the front propagation in an overdamped one-dimensional periodic lattice with the proposition of explicit continuum effective equations for finite-difference equations—which corresponds to the continuum limit with an extra spatial periodic term—and analyse directly the effective behaviour of front propagation in dissipative systems. Front propagation in finite-difference equations exhibits temporal modulation of the speed and pinning phenomena, which are contained in the continuum effective equations. This model allows the understanding of the bifurcation diagram of the front speed. Also, this description allows us to identify and characterize the particle-type solutions and their respective snaking bifurcation diagram, which we observe in the discrete systems.

## 2. Front propagation

Let us introduce a prototype model of a discrete bistable system with linear interaction or transport mechanism between first neighbour cells—the dissipative and discrete  $\phi^4$  model—which has the form

$$\frac{du_i}{dt} = \eta + \varepsilon u_i - u_i^3 + \frac{u_{i+1} - 2u_i + u_{i-1}}{(dx)^2} = -\frac{dF}{du_i}, \quad (2.1)$$

where  $F = -\sum_i \eta u_i + \varepsilon u_i^2/2 - u_i^4/4 + (u_{i+1} - u_i)^2/2dx^2$  is a Lyapunov function,  $u_i(t)$  a coarse-grained variable that accounts the dynamics on the  $i$ -cell at the instant of time  $t$ ,  $dx$  accounts for the intensity of transport between the first neighbour cells and the cell size,  $\varepsilon$  is the bifurcation parameter and  $\eta$  accounts

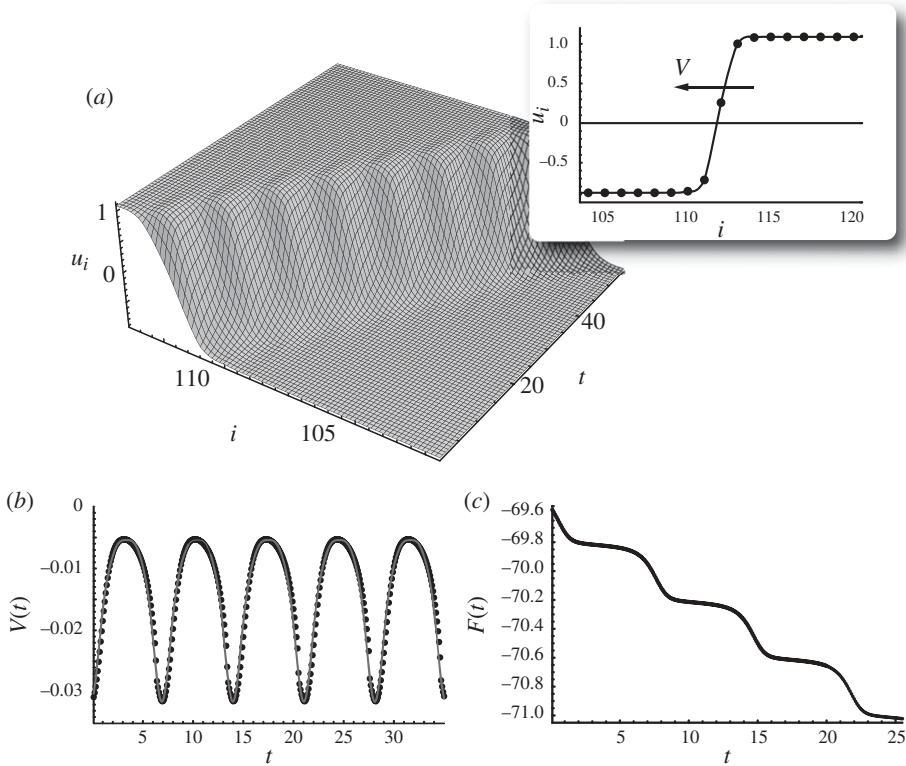


Figure 1. Front propagation. (a) Spatio-temporal diagram of front solution obtained from model (2.1) by  $\eta = 0.2$ ,  $\varepsilon = 1.0$ ,  $dt = 0.1$ , and  $dx = 2.0$ . The inset represents the front solution in a given time. (b) Dots and continuous curves are, respectively, front speed obtained by numerical simulation of model (2.1), and fitting  $V(t) = -0.014 - 0.012 \cos(\pi(t + t_0)/T) - 0.004 \cos(2\pi(t + t_0)/T) - 0.00114 \cos(3\pi(t + t_0)/T) - 0.0004 \cos(4\pi(t + t_0)/T)$  where  $t_0 = 1.8$  and  $T = 3.54$ . (c) Lyapunov potential as function of time obtained numerically from model (2.1).

for the asymmetry between the homogeneous states. The local dynamics of the previous model, near a stationary instability, describes in a unified manner the emergence of new equilibria, which is known as *the imperfect pitchfork bifurcation* [33]. The transport mechanism between first neighbour cells is linear and proportional to the difference of the coarse-grained variables in the respective cells. The model (2.1) has been used to describe propagation phenomena in various physical contexts such as nonlinear electrical lattices [34,35], individual cells in the cardiac tissue, which are resistively coupled through gap junctions (e.g. Keener [36] and references therein), in arrays of coupled nonlinear cells [37], cellular differentiation [38] and coupled chemical reactors [20].

The system (2.1) exhibits bistability in the  $\eta$ -interval  $[-2(\varepsilon/3)^{3/2}, 2(\varepsilon/3)^{3/2}]$ . In this interval model (2.1) has three uniform states, two stable and one unstable. In the case  $\eta = 0$ , the uniform states are  $u_i = \pm\sqrt{\varepsilon}$  (stable) and  $u_i = 0$  (unstable). In the bistability region for negative and large  $\eta$ , model (2.1) presents front solutions connecting asymptotically both stable states. In figure 1a is depicted the typical

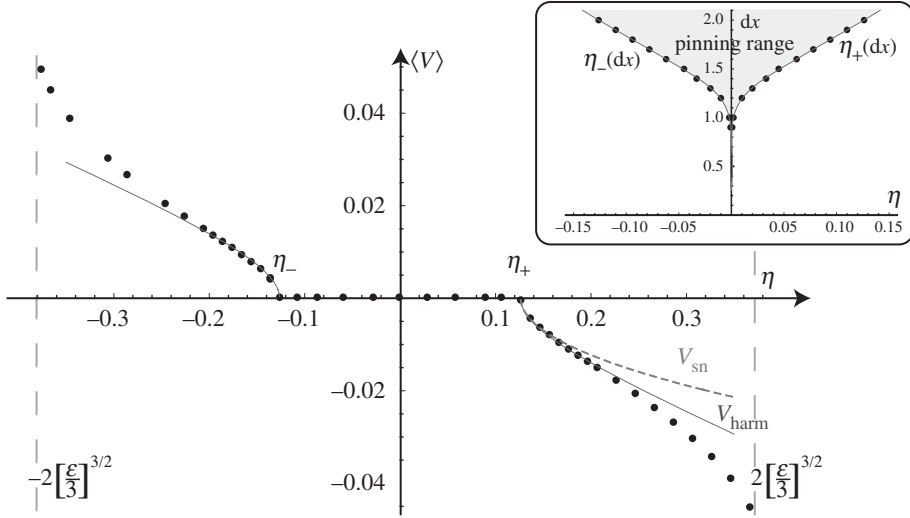


Figure 2. Average of front speed as a function of bifurcation parameter for model (2.1). The points are obtained by  $dx = 2.0$ . The vertical dashed lines represent the bistability region. The dashed and the solid curves are the average front speed obtained from the saddle-node ( $V_{sn}$ ) and harmonic approach ( $V_{harm}$ ). The inset depicts the pinning range in  $\{\eta, dx\}$ -space and the grey area is the pinning range.

front solution observed in this model. Numerically, we observe that the front speed and Lyapunov potential are periodic functions in time (cf. figure 1b,c). The negative uniform stable state invades the positive one with a oscillatory front speed. When  $\eta$  is increased the oscillatory front speed is characterized by *periodic leaps* with a large period; and when  $\eta$  is increased further suddenly at  $\eta \equiv \eta_- < 0$  the front becomes motionless, in spite of the fact that the negative state is more favourable than the positive one. This phenomenon is well known as *failure propagation*, which also originates from lattice discreteness effects [39]. Increasing  $\eta$  more until it reaches  $\eta_+ > 0$ , the front remains motionless in a range of parameter  $\eta$ -pinning range ( $[\eta_-, \eta_+]$ ). Hence, the points  $\{\eta_-, \eta_+\}$  account for points in the parameter space where the pinning–depinning transition occurs. Increasing  $\eta$  further, the positive uniform state invades the negative one with a periodic front speed, initially with a periodic leap and for large  $\eta$  with more regular oscillations. Figure 2 shows the average front speed observed for a given cell size  $dx$ . Similar pinning behaviour has been reported in an array of coupled bistable chemical reactors [20–22], a semiconductor superlattice [24] and a one-dimensional array of autocrine cells [28]. The pinning range as function of  $\eta$  and cell size is depicted in the inset of figure 2. Note that the pinning range decreases for small cell size and numerically we found the fitting  $\eta_{\pm}(dx) = \pm(2dx^{0.1} + 4dx)$ , which is represented by the continuous curve in the inset of figure 2. Then, as the cell size is smaller, the pinning region decreases by a cusp-type singularity, which is very thin for small cell size, making it difficult to observe the phenomenon of propagation failure and demonstrating that this phenomenon disappears in the continuum limit. Therefore, the pinning

region and oscillatory front propagation between homogeneous states are inherent phenomena in discrete systems.

The achieving of analytical results in this theoretical framework is in general a difficult task. To understand the rich dynamics exhibited by model (2.1), we approach this system by its continuous limit with an extra spatially periodically modulated term, which we have termed *the Peierls–Nabarro drift*. This term accounts for the intrinsic discrete nature of the system under study. The different spatial configurations of the front have different energies, which are periodic with period  $dx$  [15]. The potential that considers this energy is often denominated the Peierls–Nabarro potential. This potential was introduced in the framework of continuous theory of solid-state physics to understand the dynamics of dislocations as a result of underlying atomic lattice in the solid state [40,41] (for more thorough discussions, see [42]). On the other hand, the steady states of discrete systems and the phenomenological continuous description must be the same, and model (2.1) is invariant under spatial reflection and discrete translation with periodic  $dx$ . Therefore, we consider the simplest continuous model that includes all above ingredients, then model (2.1) is approached by the continuous equation

$$\partial_t u = \eta + \varepsilon u - u^3 + \partial_{xx} u + \Gamma_{dx}(x) \partial_{xx} u, \quad (2.2)$$

where  $\Gamma_{dx}(x) = \Gamma_{dx}(x + dx)$  is a spatial periodic function that accounts for the discrete nature of the system under study. Therefore, the last term of the above equation reveals that the interaction or the transport mechanism between the cells is characterized by the size of the cells. Recently, in the context of nonlinear optics the effect of spatial forcing on the front propagation has been studied theoretically and experimentally [43]. For zero spatial forcing ( $\Gamma_{dx}(x) = 0$ ), the above model is the continuum limit of model (2.1)—*the dissipative  $\phi^4$  model*. Therefore, the dissipative  $\phi^4$  model does not give the dynamics of the discrete system (2.1), even for infinitesimal cell size, because the dissipative  $\phi^4$  model describes only the average of front speeds. Hence, in general, we expect that the continuum limit of discrete systems loses the oscillatory nature of speed front, pinning–depinning transition phenomenon and propagation failure.

To understand the mechanisms of front propagation, we consider zero  $\eta$  and without spatial forcing the above model has kink solutions—motionless front—of the form

$$u_k(x - P) = \pm \sqrt{\varepsilon} \tanh \left( \sqrt{\frac{\varepsilon}{2}} (x - P) \right). \quad (2.3)$$

This solution links spatially the stable state  $\sqrt{\varepsilon}$  with  $-\sqrt{\varepsilon}$ , where  $P$  stands for the position of the front core, i.e. the position of the maximum of  $\partial_x u_k$ . As a result of spatial translational invariance of the  $\phi^4$  model, the kink solution is characterized by a continuous parameter  $P$ . The previous strategy for studying the effects of discreteness is based on the fact that in the limit of small  $dx$  one expects that these effects are becoming smaller. Therefore, in this limit, we can consider forcing as a perturbative term.

To study the effect of the spatial forcing and  $\eta$ , we write then the following ansatz for the front solution:

$$u(x, t) = u_k(x - P(t)) + w(x, P(t)), \quad (2.4)$$

where the position of the front core  $P(t)$  has been promoted to a slowly varying function of time in order to account for the periodic forcing and energy asymmetry between the equilibrium states, and  $w$  is a small correction that is of the order of  $\dot{P} \ll 1$ . The dynamic equation of  $P$  characterizes the evolution of the front solution. Introducing the above ansatz in the effective equation (2.1) and linearizing in  $w$ , we obtain

$$\mathcal{L}w = -\dot{P}\partial_z u_k - \eta - \Gamma_{\text{dx}}(x)\partial_{zz}u_k, \quad (2.5)$$

where the linear operator  $\mathcal{L} \equiv \partial_{zz} + \varepsilon - 3u_k^2(z)$ , and  $z = x - P$  is the moving coordinate. Considering the inner product  $\langle f | g \rangle \equiv \int_{-\infty}^{\infty} fg \, dx$ , the linear operator  $\mathcal{L}$  is self-adjoint ( $\mathcal{L}^\dagger = \mathcal{L}$ ). The kernel of this operator is characterized by the goldstone mode  $\partial_z u_k$ , which is  $\mathcal{L}^\dagger \partial_z u_k = 0$ . In order to have a solution of the linear equation (2.5), the right-hand side of equation (2.5) has to be orthogonal to the kernel elements of  $\mathcal{L}^\dagger$ ; therefore, we have to impose the following solvability condition, which is also called the Fredholm alternative (see [4]):

$$\dot{P} = \frac{-3\eta}{\sqrt{2\varepsilon}} + \gamma_{\text{dx}}(P) \equiv \frac{-3\eta}{\sqrt{2\varepsilon}} - \frac{\int_{-\infty}^{\infty} dz \partial_z u_k \Gamma_{\text{dx}}(z + P) \partial_{zz} u_k}{\int_{-\infty}^{\infty} dz (\partial_z u_k)^2}. \quad (2.6)$$

Hence, the front speed is constituted by two drifts, a constant ( $-3\eta/\sqrt{2\varepsilon}$ ) and periodic ones, which are related to the energy difference of two states and the discrete nature of the system under study ( $\gamma_{\text{dx}}(P + dx) = \gamma_{\text{dx}}(P)$ ), respectively. In the range of parameters where the value of the constant part is smaller than the amplitude of the periodic one, the front is motionless—pinning range. Note that this dynamical behaviour is independent of the energy difference of the uniform states. In this parameter region, the system has infinite equilibria, which correspond to a rigid translation of the kink solution.

### (a) Pinning–depinning transition

When the value of the constant drift is close to the amplitude of the periodic one ( $\eta \sim \eta_{\pm}$ , for the sake of simplicity without loss of generality we consider  $\eta \sim \eta_+$ ), the dynamics around the equilibria is approached by a saddle-node bifurcation, i.e.

$$\dot{P} \approx \sigma(\eta - \eta_+) - \alpha P^2. \quad (2.7)$$

The last approach is based on the separation of scale that displays the position of the front near and far from the region where the equilibrium points are created. The slower dynamics drives the evolution of the front, which corresponds to the region where the equilibrium points appear. For  $\eta < \eta_+$ ,  $P$  has equilibrium points that account for the different positions of the stationary front. When  $\eta = \eta_+$ , the equilibrium positions disappear by saddle-node bifurcation and the system presents a pinning–depinning transition. Finally, for  $\eta > \eta_+$ , the front speed is characterized by periodic leaps. From the approach (2.7), we can estimate the average front speed based on bottleneck time (cf. [33]), that is, one can estimate the average speed of the front considering the distance between cells

and the time spent around the region where the equilibrium points disappear, and it reads

$$V_{\text{sn}} \approx dx \sqrt{\frac{\sigma(\eta - \eta_+)}{\alpha}}. \quad (2.8)$$

Hence, the average front speed increases as the square root of  $\eta$  around the critical value  $\eta_+$ . This average speed,  $V_{\text{sn}}$ , is depicted by the dashed curve in figure 2 and it is in quite good agreement close to  $\eta_+$ . An analogous result can be deduced around  $\eta_-$ .

(b) *Average front speed*

To study the dynamics far from the saddle-node bifurcation for the sake of simplicity, we have considered a simple harmonic approach by

$$\gamma(P) \approx \gamma_0 \sin\left(\frac{2\pi P}{dx}\right). \quad (2.9)$$

In this case, we have  $\eta_{\pm} = \pm\sqrt{2}\varepsilon\gamma_0/3$ . Then we integrate equation (2.6) and obtain the following analytical expression:

$$P(t) = P_0 + \frac{dx}{2\pi} \arctan \left[ \tan \left( \frac{dx}{2\pi\sqrt{9\eta^2/\gamma_0^2 2\varepsilon^2 - 1}} t \right) \frac{\sqrt{3\eta + \gamma_0\sqrt{2\varepsilon^2}}}{\sqrt{3\eta - \gamma_0\sqrt{2\varepsilon^2}}} \right]. \quad (2.10)$$

The above expression can be rewritten in the following form:

$$\tan \left[ \frac{2\pi(P(t) - P_0)}{dx} \right] = \frac{\sqrt{3\eta + \gamma\sqrt{2\varepsilon^2}}}{\sqrt{3\eta - \gamma\sqrt{2\varepsilon^2}}} \tan \left( \frac{dx}{2\pi\sqrt{9\eta^2/\gamma^2 2\varepsilon^2 - 1}} t \right), \quad (2.11)$$

hence, we have the equality of two periodic functions of period  $2\pi$ . If  $\lambda$  and  $\tau$  are, respectively, the spatial and temporal periods, then they satisfy the relation

$$\lambda = dx \quad \text{and} \quad \tau = \mp \frac{\sqrt{9\eta^2/\gamma^2 2\varepsilon^2 - 1}}{dx},$$

and the average front speed can be defined as

$$V_{\text{harm}} = \frac{\lambda}{\tau} = \mp \sqrt{\frac{9\eta^2}{\gamma^2 2\varepsilon^2 - 1}}. \quad (2.12)$$

As an alternative way, we can rewrite the above expression as [44]

$$V_{\text{harm}} = dx \sqrt{\left(\frac{\eta}{\eta_{\pm}}\right)^2 - 1}. \quad (2.13)$$

For  $|\eta| < |\eta_{\pm}|$ , the above formula is imaginary, i.e. the front speed is zero. Close to  $\eta_{\pm}$ , the above formula recovers the dynamical behaviour expected for a

saddle-node bifurcation, with the front speed increasing as the square root of  $\eta$ , as predicted by the following formula:

$$V_{\text{harm}} \approx dx \sqrt{\frac{2(\eta - \eta_{\pm})}{\eta_{\pm}}}. \quad (2.14)$$

However, for large  $\eta$ , the average front speed behaves as a linear function of  $\eta$ , which is consistent with the front speed obtained by the standard continuum description ( $\Gamma_{dx} = 0$ ,  $V \approx -3\eta/\sqrt{2\varepsilon}$ ). Figure 2 shows the  $V_{\text{harm}}$  by a solid curve, which is in quite good agreement with the numerical results obtained by finite-difference equation (2.1) with  $dx = 2.0$ . Hence, the dynamics of finite-difference equation (2.1) is well described by a simple harmonic periodic drift in model (2.2).

### 3. Front interaction and localized states

Apart from the understanding of the front propagation in finite-difference equations, the effective continuum equations enable us to describe unexpected dynamics of particle-like solutions. Based on front interaction and small  $\eta$ , we can consider the following ansatz for the kink and anti-kink interactions [45]:

$$u = u_k \left( x - \frac{\Delta}{2} \right) - u_k \left( x + \frac{\Delta}{2} \right) - \sqrt{\varepsilon} + w(x, \Delta), \quad (3.1)$$

where  $\Delta$  is a slowly varying variable that accounts for the distance between the core of the fronts. In figure 3 is outlined the above ansatz. Introducing the above ansatz in equation (2.2) and linearizing in  $w$ , we obtain analogously a linear equation that has a solution if it satisfies the following solvability condition:

$$\dot{\Delta} = f(\Delta) = -\frac{6\eta}{\sqrt{2\varepsilon}} + 2\gamma_{dx}(\Delta) - \beta e^{-\sqrt{\varepsilon}\Delta}, \quad (3.2)$$

where

$$\beta \equiv 6 \frac{\int dz \partial_z u_k(z) u_k^2(z) e^{-\sqrt{\varepsilon}z}}{\int dz (\partial_z u_k(z))^2}$$

is a positive number. Hence, the front interaction is characterized by the superposition of a constant drift, a periodic and an attractive exponential ‘force’. Close to the Maxwell point,  $\eta = 0$ , the system has infinite equilibria,  $f(\Delta^*) = 0$ , that are stable if  $f'(\Delta^*) < 0$ . Each one corresponds to different localized states. Thus, the existence and the stability of localized states are given by the oscillatory nature of the front interaction, which is a result of the discrete nature of the system under study. The lengths of the localized state are roughly multiples of the cell size. Numerical simulations of the discrete equation (2.1) show the existence of the solutions predicted by equation (3.1). Figure 4a depicts the front interaction law. Examples of localized states are shown in the insets. Changing  $\eta$ , the localized structures disappear by a sequence of successive saddle-node bifurcations (see [45] and references therein). Hence, the system exhibits coexistence of different branches of localized states in the parameter space characterized by the snaking bifurcation [46,47]. The snaking bifurcation diagram obtained from model (2.1)

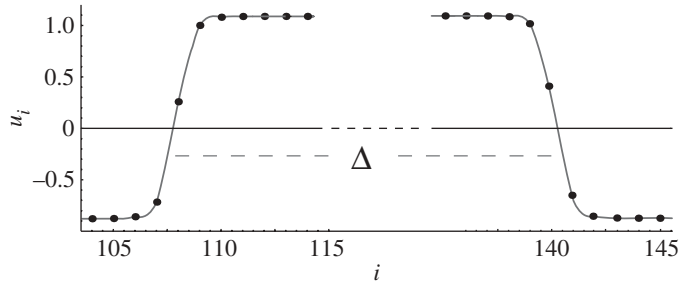


Figure 3. Schematic of the interaction of kink and anti-kink solutions.

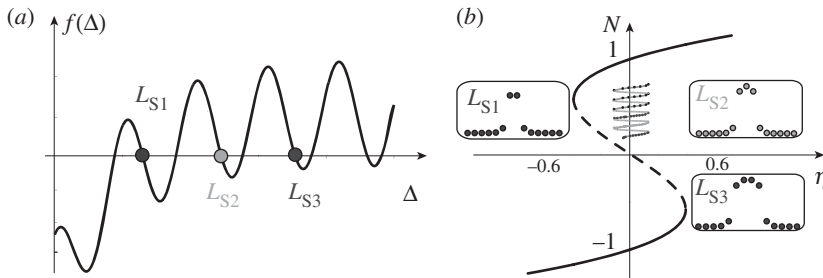


Figure 4. Localized states of finite-difference model (2.1). (a) Schematic of front interaction, formula (3.1). The circle symbols stand for stable localized states ( $L_{S_i}$ ,  $i = 1, 2, \dots$ ). Inset figures depict the different localized states. (b) Snaking bifurcation diagram obtained from model (2.1) by  $dx = 2.0$ ; the horizontal axis is  $\eta$ -parameter, the vertical axis is the norm,  $N = \sum_i (u_i + \varepsilon)$ , and S-shape is the uniform states of model (2.1) as a function of  $\eta$ .

is depicted in figure 4b. Therefore, the localized states and their respective organization in the space of parameters are fully described by the continuous phenomenological equation (2.2).

### 4. Conclusions

Mesoscopic and macroscopic spatially extended systems are often described by their continuum limit; however, interface propagation in an overdamped one-dimensional periodic lattice leads to different conclusions in the discrete and continuous description, and phenomenological continuum equations allow us to grasp the observed dynamical behaviours of their respective discrete systems. Hence, one has an adequate framework to understand novel phenomena and to achieve analytical results in finite-difference equations. Propagation of fronts in higher dimensions in discrete systems should exhibit similar phenomena to those we observed, which can account for complex and unexpected behaviours (e.g. [48]); a study in this direction is in progress.

We can consider more generic Peierls–Nabarro drift terms in the phenomenological continuous description of the form  $\Gamma_{dx}(x, \partial_x u) \partial_{xx} u$ ; however, we obtain similar results to those obtained with the simplest continuous description.

A pinning–depinning transition similar to that shown in figure 2 has also been observed for travelling waves in the context of coupled map lattices, when the parameter that describes the advective speed is changed. This phenomenon of failure propagation can be understood as an effect of spatial discretization. Work in this direction is in progress.

The simulation software *DIMX*, developed at INLN France, has been used for all numerical simulations presented in this paper. M.G.C. and R.G.R. acknowledge, respectively, the financial support of FONDECYT projects 1090045 and 11080286.

## References

- 1 Flach, S. & Willis, C. R. 1998 Discrete breathers. *Phys. Rep.* **295**, 181–264. (doi:10.1016/S0370-1573(97)00068-9)
- 2 Newell, A. C. 1985 *Solitons in mathematics and physics*. Philadelphia, PA: Society for Industrial and Applied Mathematics.
- 3 Murray, J. D. 1993 *Mathematical biology*. Berlin, Germany: Springer.
- 4 Pismen, L. M. 2006 *Patterns and interfaces in dissipative dynamics*. Springer Series in Synergetics. Berlin, Germany: Springer.
- 5 Fisher, R. A. 1937 The wave of advance of advantageous genes. *Ann. Eugen.* **7**, 355–369.
- 6 Kolmogorov, A. N., Petrovsky, I. G. & Piskunov, N. S. 1937 Etude de l'équation de la diffusion avec croissance de la quantité de matière et son application à un problème biologique. *Bull. Univ. d'Etat à Moscou, Sér. Int. A* **1**, 1–25.
- 7 Cross, M. C. & Hohenberg, P. C. 1993 Pattern formation outside of equilibrium. *Rev. Mod. Phys.* **65**, 851–1112. (doi:10.1103/RevModPhys.65.851)
- 8 Clerc, M. G., Nagaya, T., Petrossian, A., Residori, S. & Riera, C. 2004 First-order Fréedericksz transition and front propagation in a liquid crystal light valve with feedback. *Eur. Phys. J. D* **28**, 435–445. (doi:10.1140/epjd/e2003-00316-1)
- 9 Residori, S., Petrossian, A., Nagaya, T., Riera, C. & Clerc, M. G. 2004 Fronts and localized structures in a liquid-crystal-light-valve with optical feedback. *Physica D* **199**, 149–165. (doi:10.1016/j.physd.2004.08.010)
- 10 Goldstein, R. E., Gunaratne, G. H., Gil, L. & Coulet, P. 1991 Hydrodynamic and interfacial patterns with broken space–time symmetry. *Phys. Rev. A* **43**, 6700–6721. (doi:10.1103/PhysRevA.43.6700)
- 11 Pomeau, Y. 1986 Front motion, metastability and subcritical bifurcations in hydrodynamics. *Physica D* **23**, 3–11. (doi:10.1016/0167-2789(86)90104-1)
- 12 Clerc, M. G., Falcon, C. & Tirapegui, E. 2005 Additive noise induces front propagation. *Phys. Rev. Lett.* **94**, 148302. (doi:10.1103/PhysRevLett.94.148302)
- 13 Clerc, M. G., Falcon, C. & Tirapegui, E. 2006 Front propagation sustained by additive noise. *Phys. Rev. E* **74**, 011303. (doi:10.1103/PhysRevE.74.011303)
- 14 Ishimori, Y. & Munakata, T. 1982 Kink dynamics in the discrete Sine–Gordon system a perturbational approach. *J. Phys. Soc. Jpn* **51**, 3367–3374. (doi:10.1143/JPSJ.51.3367)
- 15 Peyrard, M. & Kruskal, M. D. 1984 Kink dynamics in the highly discrete sine–Gordon system. *Physica D* **14**, 88–102. (doi:10.1016/0167-2789(84)90006-X)
- 16 Karpan, V. M., Zolotaryuk, Y., Christiansen, P. L. & Zolotaryuk, A. V. 2002 Discrete kink dynamics in hydrogen-bonded chains: the one-component model. *Phys. Rev. E* **66**, 066603. (doi:10.1103/PhysRevE.66.066603)
- 17 Dawson, S. P., Keizer, J. & Pearson, J. E. 1999 Fire-diffuse-fire model of dynamics of intracellular calcium waves. *Proc. Natl Acad. Sci. USA* **96**, 6060–6063. (doi:10.1073/pnas.96.11.6060)
- 18 Bugrim, A. E., Zhabotinsky, A. M. & Epstein, I. R. 1997 Calcium waves in a model with a random spatially discrete distribution of  $\text{Ca}^{2+}$  release sites. *Biophys. J.* **73**, 2897–2906. (doi:10.1016/S0006-3495(97)78318-8)

- 19 Keizer, J., Smith, G. D., Ponce-Dawson, S. & Pearson, J. E. 1998 Saltatory propagation of  $\text{Ca}^{2+}$  waves by  $\text{Ca}^{2+}$  sparks. *Biophys. J.* **75**, 595–600. (doi:10.1016/S0006-3495(98)77550-2)
- 20 Laplante, J. P. & Erneux, T. 1992 Propagation failure in arrays of coupled bistable chemical reactors. *J. Phys. Chem.* **96**, 4931–4934. (doi:10.1021/j100191a038)
- 21 Laplante, J. P. & Erneux, T. 1992 Propagation failure and multiple steady states in an array of diffusion coupled flow reactors. *Physica A* **188**, 89–98. (doi:10.1016/0378-4371(92)90256-P)
- 22 Booth, V., Erneux, T. & Laplante, J. P. 1994 Experimental and numerical study of weakly coupled bistable chemical reactors. *J. Phys. Chem.* **98**, 6537–6540. (doi:10.1021/j100077a019)
- 23 Löcher, M., Cigna, D. & Hunt, E. R. 1998 Noise sustained propagation of a signal in coupled bistable electronic elements. *Phys. Rev. Lett.* **80**, 5212–5215. (doi:10.1103/PhysRevLett.80.5212)
- 24 Amann, A. & Schöll, E. 2005 Bifurcations in a system of interacting fronts. *J. Stat. Phys.* **119**, 1069–1138. (doi:10.1007/s10955-005-4405-2)
- 25 Cole, W. C., Picone, J. B. & Sperelakis, N. 1988 Gap junction uncoupling and discontinuous propagation in the heart. A comparison of experimental data with computer simulations. *Biophys. J.* **53**, 809–818. (doi:10.1016/S0006-3495(88)83160-6)
- 26 Keener, J. P. 1991 The effects of discrete gap junction coupling on propagation in myocardium. *J. Theor. Biol.* **148**, 49–82. (doi:10.1016/S0022-5193(05)80465-5)
- 27 deCastro, M., Hofer, E., Muñuzuri, A. P., Gómez-Gesteira, M., Plank, G., Schafferhofer, I., Pérez-Muñuzuri, V. & Pérez-Villar, V. 1999 Comparison between the role of discontinuities in cardiac conduction and in a one-dimensional hardware model. *Phys. Rev. E* **59**, 5962–5969. (doi:10.1103/PhysRevE.59.5962)
- 28 Muratov, C. B. & Shvartsman, S. Y. 2004 Signal propagation and failure in discrete autocrine relays. *Phys. Rev. Lett.* **93**, 118101. (doi:10.1103/PhysRevLett.93.118101)
- 29 Ustinov, A. V., Doderer, T., Vernik, I. V., Pedersen, N. F., Huebener, R. P. & Oboznov, V. A. 1993 Experiments with solitons in annular Josephson junctions. *Physica D* **68**, 41–44. (doi:10.1016/0167-2789(93)90026-W)
- 30 Christodoulides, D. N. & Joseph, R. I. 1988 Discrete self-focusing in nonlinear arrays of coupled waveguides. *Opt. Lett.* **13**, 794–796. (doi:10.1364/OL.13.000794)
- 31 McLaughlin, D., Shapley, R., Shelley, M. & Wielaard, D. J. 2000 A neuronal network model of macaque primary visual cortex (V1): orientation selectivity and dynamics in the input layer 4Ca. *Proc. Natl Acad. Sci. USA* **97**, 8087–8092. (doi:10.1073/pnas.110135097)
- 32 Fáth, G. 1998 Propagation failure of traveling waves in a discrete bistable medium. *Physica D* **116**, 176–190. (doi:10.1016/S0167-2789(97)00251-0)
- 33 Strogatz, S. H. 1994 *Nonlinear dynamics and chaos: with applications to physics, biology, chemistry and engineering*. Reading, MA: Addison-Wesley.
- 34 Marquie, P., Binczak, S., Comte, J. C., Michaux, B. & Bilbault, J. M. 1998 Diffusion effects in a nonlinear electrical lattice. *Phys. Rev. E* **57**, 6075–6078. (doi:10.1103/PhysRevE.57.6075)
- 35 Remoissenet, M. 1999 *Waves called solitons: concepts and experiments*. Berlin, Germany: Springer.
- 36 Keener, J. P. 2000 Homogenization and propagation in the bistable equation. *Physica D* **136**, 1–17. (doi:10.1016/S0167-2789(99)00151-7)
- 37 Kladko, K., Mitkov, I. & Bishop, A. R. 2000 Universal scaling of wave propagation failure in arrays of coupled nonlinear cells. *Phys. Rev. Lett.* **84**, 4505–4508. (doi:10.1103/PhysRevLett.84.4505)
- 38 Fáth, G. & Ski, Z. D. 1999 Avalanche of bifurcations and hysteresis in a model of cellular differentiation. *Phys. Rev. E* **66**, 4604–4609. (doi:10.1103/PhysRevE.60.4604)
- 39 Keener, J. P. 1987 Propagation and its failure in coupled systems of discrete excitable cells. *SIAM J. Appl. Math.* **47**, 556–572. (doi:10.1137/0147038)
- 40 Peierls, R. F. 1940 The size of a dislocation. *Proc. Phys. Soc.* **52**, 34–37. (doi:10.1088/0959-5309/52/1/305)
- 41 Nabarro, F. R. N. 1947 Dislocations in a simple cubic lattice. *Proc. Phys. Soc.* **59**, 256–272. (doi:10.1088/0959-5309/59/2/309)
- 42 Nabarro, F. R. N. 1987 *Theory of crystal dislocations*. New York, NY: Dover.

- 43 Haudin, F., Elias, R. G., Rojas, R. G., Bortolozzo, U., Clerc, M. G. & Residori, S. 2009 Driven front propagation in 1D spatially periodic media. *Phys. Rev. Lett.* **103**, 128003. (doi:10.1103/PhysRevLett.103.128003)
- 44 Rojas, R. 2005 Sur de gouttes, cristaux liquides et fronts. PhD thesis, University of Nice Sophia Antipolis, France. See <http://tel.archives-ouvertes.fr>.
- 45 Clerc, M. G. & Falcon, C. 2005 Localized patterns and hole solutions in one-dimensional extended systems. *Physica A* **356**, 48–53. (doi:10.1016/j.physa.2005.05.011)
- 46 Woods, P. D. & Champneys, A. R. 1999 Heteroclinic tangles and homoclinic snaking in the unfolding of a degenerate reversible Hamiltonian–Hopf bifurcation. *Physica D* **129**, 147–170. (doi:10.1016/S0167-2789(98)00309-1)
- 47 Bortolozzo, U., Clerc, M. G. & Residori, S. 2008 Local theory of the slanted homoclinic snaking bifurcation diagram. *Phys. Rev. E* **78**, 036214. (doi:10.1103/PhysRevE.78.036214)
- 48 Rojas, R. G., Elias, R. G. & Clerc, M. G. 2009 Dynamics of an interface connecting a stripe pattern and a uniform state: amended Newell–Whitehead–Segel equation. *Int. J. Bifurcat. Chaos* **19**, 2801–2812. (doi:10.1142/S0218127409024499)